

Obtaining attosecond x-ray pulses using a self-amplified spontaneous emission free electron laser

A. A. Zholents and G. Penn

Lawrence Berkeley National Laboratory, Berkeley, California 94720, USA

(Received 13 January 2005; published 24 May 2005)

We describe a technique for the generation of a solitary attosecond x-ray pulse in a free-electron laser (FEL), via a process of self-amplified spontaneous emission. In this method, electrons experience an energy modulation upon interacting with laser pulses having a duration of a few cycles within single-period wiggler magnets. Two consecutive modulation sections, followed by compression in a dispersive section, are used to obtain a single, subfemtosecond spike in the electron peak current. This region of the electron beam experiences an enhanced growth rate for FEL amplification. After propagation through a long undulator, this current spike emits a ~ 250 attosecond x-ray pulse whose intensity dominates the x-ray emission from the rest of the electron bunch.

DOI: 10.1103/PhysRevSTAB.8.050704

PACS numbers: 41.60.Cr, 29.27.-a

I. METHOD

Various ideas for the generation of attosecond x-ray pulses using free-electron lasers (FELs) have been published recently [1–5]. Here, we expand on an idea briefly described in Ref. [5].

Figure 1 shows a schematic of the proposed technique. On the left, the electron beam exits the linac and enters two adjacent wiggler magnets, labeled W1 and W2, where each magnet has just one wiggler period. Two copropagating laser pulses enter the wigglers at a small angle, ϕ . The carrier wave frequencies of these lasers are chosen to be in the ratio of 4:3. The first laser pulse is focused in the center of the first wiggler and the second laser pulse is focused in the center of the second wiggler. Each laser interacts with the same group of electrons at its focal point. These pulses consist of only a small number of optical cycles. For the first laser pulse, the phase of the carrier wave is adjusted so that the electric field is zero when the peak of the laser pulse envelope reaches the center of the first wiggler. A snapshot of the laser electric field at this moment is shown in Fig. 2(a) for a laser pulse of 7.5 fs (FWHM of intensity) and a wavelength of 1200 nm. The FWHM of the laser intensity corresponds to only 1.9 laser periods. The phase of the carrier wave of the second laser pulse is adjusted so that the electric field is zero when the peak of the laser pulse envelope reaches the center of the second wiggler. A snapshot of the laser electric field at this moment is shown in Fig. 2(b) for a 10 fs laser pulse at 1600 nm wavelength. A technique for obtaining such pulses using an optical parametric amplifier is described elsewhere [6–9].

For each wiggler, the wiggler parameter $K = eB_0\lambda_w/2\pi mc$ (where λ_w is the wiggler period, B_0 is the peak magnetic field, e and m are the electron charge and mass, and c is the speed of light) is adjusted to maximize the amplitude of the energy modulation generated within an electron beam by a laser pulse focused in the center of that wiggler. We calculate this energy modulation using the following FEL equation [10,11]:

$$\begin{aligned} \frac{d\gamma(\hat{s})}{d\hat{z}} = & \sqrt{16\pi \frac{A}{\tau P_0} N \xi [J_0(\xi/2) - J_1(\xi/2)]} \\ & \times \sqrt{\frac{q}{1 + (q\hat{z})^2}} \cos \left[2\pi\nu\hat{z} + \arctan(q\hat{z}) - 2\pi N\hat{s} - \frac{\pi}{2} \right. \\ & \left. - \frac{x_0^2 \sin^2(2\pi\hat{z})}{1 + (q\hat{z})^2} \right] e^{-x_0^2 \sin^2(2\pi\hat{z})/[1 + (q\hat{z})^2]} e^{-(\hat{z}-\hat{s})^2/2\sigma_s^2}, \end{aligned} \quad (1)$$

where A is the laser pulse energy; $\xi = K^2/(2 + K^2)$, J_0, J_1 are zero and first order Bessel functions of the first kind; $P_0 = I_A mc^2/e \approx 8.7 \times 10^9$ W and I_A is the Alfvén current; N is the number of wiggler periods, and we use $N = 1$; $q = N\lambda_w/Z_R$ and Z_R is the Rayleigh length. The scaled coordinates are $\hat{z} = z/(N\lambda_w)$ where z is the coordinate along the wiggler, and $\hat{s} = s/(N\lambda)$ where s is the coordinate along the electron beam; also, $\sigma_s = \sqrt{2}c\tau/(2.35N\lambda)$ where τ is the duration of the laser pulse in terms of FWHM of intensity. The wiggler detuning parameter $\nu = N\Delta\lambda/\lambda$, corresponding to $\Delta\lambda = \lambda_r - \lambda$, where λ is the laser wavelength, $\lambda_r = \lambda_w[1 + K^2/2 + (\gamma\phi)^2]/2\gamma^2$ is the FEL resonance wavelength, and γ is the electron relativistic factor. The amplitude of the orbit of the electron beam in the wiggler normalized to the laser spot size w_0 is $x_0 = K\lambda_w/(2\pi\gamma w_0)$, where the laser spot size at the wiggler

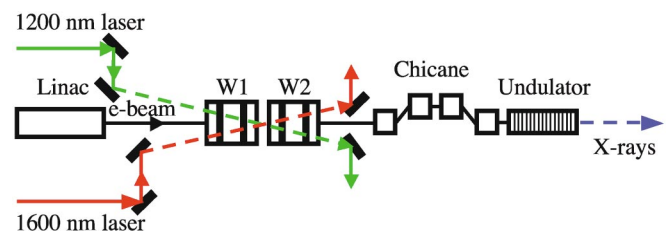


FIG. 1. (Color) A schematic of the components involved in attosecond x-ray pulse production.

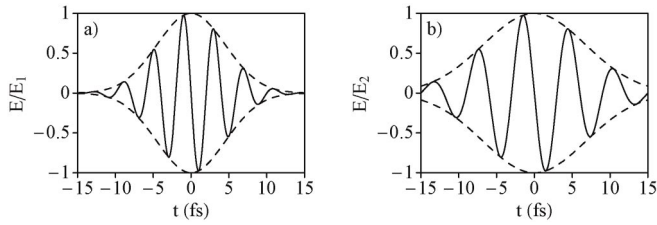


FIG. 2. A snapshot of the laser electric field normalized to the peak value: (a) 1200 nm laser wavelength and 7.5 fs pulse (FWHM of intensity); (b) 1600 nm laser wavelength and 10 fs pulse.

center is defined by $w_0^2 = Z_R \lambda / \pi$, which is assumed to be larger than the electron beam size.

Following [12], we note that the function

$$f(\nu, q) = \int_{-0.5}^{0.5} d\hat{z} \sqrt{\frac{q}{1 + (q\hat{z})^2}} \cos[2\pi\nu\hat{z} + \arctan(q\hat{z})], \tag{2}$$

reaches a smooth maximum at $q \approx 4$ and $\nu \approx -0.5$ (see Fig. 3). This function essentially characterizes the amplitude of energy modulation attainable in accordance with Eq. (1). Thus, we use these values for q and ν in all remaining calculations.

The interaction of the electron beam with the two laser fields in the two wigglers results in a complex time-dependent energy modulation of the electrons. The energy modulation produced by the first laser pulse alone with pulse energy $A = 0.2$ mJ and duration $\tau = 7.5$ fs, in a wiggler with $\lambda_w = 70$ cm and $K = 73$ ($\gamma \approx 28000$), is shown in Fig. 4(a). The above laser parameters have not yet been demonstrated experimentally. The energy modulation produced by the second laser pulse alone with $A = 0.07$ mJ, $\tau = 10$ fs, in a wiggler with the same wiggler period but $K = 85$, is similar but with lower amplitude and a longer length scale. A time delay between two laser pulses is adjusted such as to overlap the actions of the two lasers where the gradient of the energy modulation is at a maximum. This is the longitudinal coordinate denoted as zero in Fig. 4(a). The resulting, combined energy modulation is shown in Fig. 4(b). Because the laser wavelength of the second laser is longer than that of the first laser, both modulations work to increase the central peak, while the two modulations counter each other at adjacent side peaks,

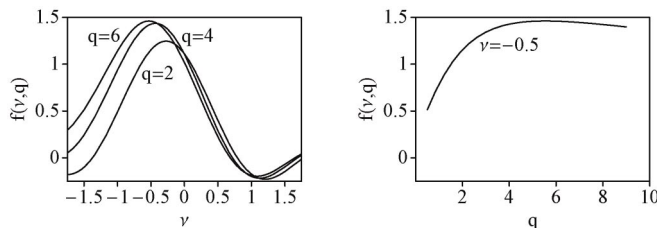


FIG. 3. Function $f(\nu, q)$.

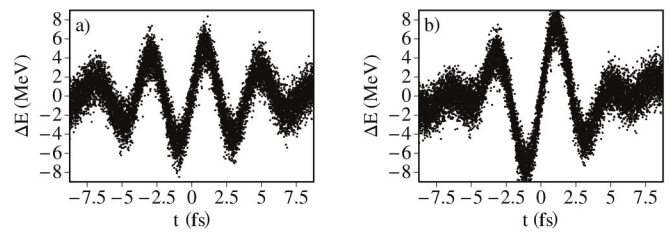


FIG. 4. (a) The calculated energy modulation of the electrons along the electron bunch produced in the interaction with a few-cycle, 1200 nm laser pulse in the wiggler magnet; (b) the combined energy modulation from a few-cycle, 1200 nm laser pulse in one wiggler magnet, and a few-cycle, 1600 nm laser pulse in a second wiggler magnet.

reducing the combined modulation at this longitudinal position. We choose the maximum amplitude for the second energy modulation to be one half of the amplitude of the first modulation. In this case, the side peaks adjacent to the central peak are significantly reduced and later peaks are sufficiently small as to have no appreciable effect.

Each of the two laser pulses described above has a relative frequency bandwidth of 24% FWHM, which is near the limit of current laser technology. If only one such laser were used, the secondary peaks in electric field would produce an energy modulation that is 65% as large as that of the central peak, which is not sufficiently different to provide a strong contrast for the central peak in FEL output. The distinct energy modulation produced by superimposing the two laser-electron beam interactions mimics a larger effective bandwidth centered between the two laser frequencies. The superposition of the two energy modulations follows a modulated waveform envelope which is partially “pinched” two laser periods from the center of the envelope, as shown in Fig. 5. Note that even though the waveform envelope is not reduced to zero at the location of

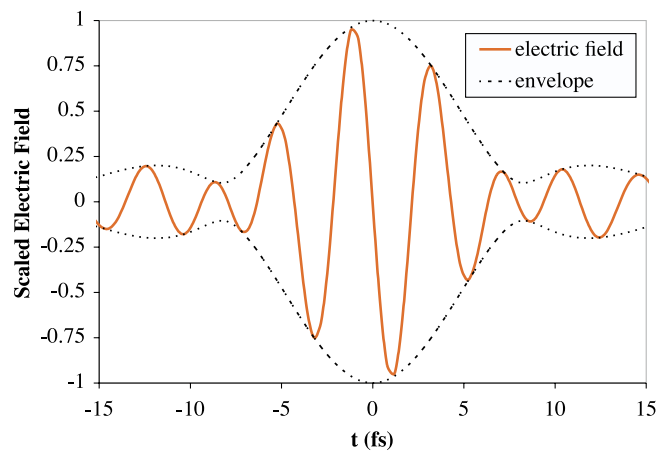


FIG. 5. (Color) The electric field of the two lasers as a function of time, superimposed where the electric field from each laser vanishes at the midpoint. The envelope of the waveform is also shown (dashed line).

the secondary peaks in energy modulation, the width of the envelope is significantly reduced. The amplitude of the electric field remains below 1/5 of the peak value for all but the central 10 fs of the laser waveform.

After modulation, the electron beam passes through a dispersive magnetic chicane where higher energy electrons travel a shorter path and lower energy electrons travel a longer path. The chicane is chosen to have dispersion parameter $R_{56} = 540 \mu\text{m}$. This produces a microbunching of the electrons and enhancement of the electron peak current. We will demonstrate below that the current enhancement produced in the central cycle of the two laser pulses is much stronger than the current enhancement produced during other laser cycles.

II. REDUCTION IN GAIN LENGTH

After bunching by means of the chicane, the electron beam enters the long undulator with undulator period and undulator parameter matched to produce radiation at the x-ray wavelength λ_x via the process of self-amplified spontaneous emission (SASE) (see [13] and references therein for a description of SASE). Naturally, we expect electrons at the central current peak to experience enhanced SASE with shorter gain length because of the local current enhancement.

The choice of electron beam and undulator parameters is stimulated by the design report for the Linac Coherent Light Source (LCLS) [14], i.e., the average beam current I_0 is 3.4 kA, the beam energy is 14 GeV, the energy spread is 1.1 MeV, the normalized emittance is $1.2 \mu\text{m}$, and the average beta function is 18 m. The output radiation has wavelength $\lambda_x = 0.15 \text{ nm}$.

After bunching, the peak value of the current becomes 18 kA. A preliminary examination of possible deleterious effects from the enhanced peak current has been reported on in Ref. [15]. The most significant cause for concern is the longitudinal space charge forces. For the given parameters, the electrons sit within a pencil-like beam in their rest frame, and the free-space impedance from longitudinal space charge can be approximated as [16]:

$$Z(k) \simeq i \frac{Z_0}{4\pi} \frac{k}{\gamma^2} \left(1 + 2 \ln \frac{\gamma}{kr_b} \right), \quad (3)$$

where k is the wave number of the perturbation, $Z_0 = 377 \Omega$ is the vacuum impedance, $\gamma \simeq 28000$, and r_b is the radius of the electron beam. While this expression has been derived for beam lines containing only drift sections and focusing elements, we apply it without modification to the present case where the electron beam is passing through the undulator and oscillates almost rigidly with a deviation of less than $1 \mu\text{m}$.

The enhanced current has a roughly Gaussian profile, with standard deviation $\sigma_z \simeq 50 \text{ nm}$. In calculating the wakefield per unit length $W(z)$, close to the microbunch it is a good approximation to take $k \rightarrow 1/\sigma_z$ in the loga-

rithm term. The wakefield then simplifies to

$$W(z) \simeq \frac{Z_0}{8\pi} I_{\text{peak}} \frac{1}{\sigma_z \gamma^2} \left(1 + 2 \ln \frac{\gamma \sigma_z}{r_b} \right) \frac{z}{\sigma_z} \exp\left(-\frac{z^2}{2\sigma_z^2}\right). \quad (4)$$

The maximum of the wakefield occurs at $\pm \sigma_z$, and for the given parameters it equals $\pm 0.024 \text{ MeV/m}$. As a result, longitudinal space charge yields a chirplike variation in energy, and after 50 m of propagation through undulators, a swing in energy of 2.4 MeV over 0.3 fs is produced. For comparison, the SASE process itself generates an energy spread of up to 7 MeV after 50 m, and the energy bandwidth for the SASE process is expected to be about 50 MeV.

For a quantitative analysis of the output from SASE, we first use a 3D model from Ref. [17] and the fitting formula derived there. Using the above electron beam parameters, we calculate that the gain length for the central current peak is approximately 40% shorter than the gain length for the side peaks and approximately a factor of 2 shorter than the gain length for electrons in the electron beam outside of the modulation region. Therefore, when the central peak radiation reaches saturation, which occurs after the electron beam propagates through the undulator for approximately eight gain lengths, the radiation of the side peaks is far from saturation reaching only approximately 1/40 of the intensity of the central peak radiation. The radiation of electrons outside of the modulation region is even weaker. If one stops SASE here by providing, for example, a slight distortion of the electron beam trajectory, then the x-ray signal in the experimental area outside of the undulator will appear as a solitary x-ray pulse sitting a top of a low intensity pedestal. We refer to this pulse as the attosecond x-ray pulse (AXP).

Because of the fact that the AXP is generated via the interaction of electrons with the laser pulses, there is an absolute synchronization between the AXP and the lasers. However, to make full use of it, the relative timing jitter between the arrival time of the electron beam and the laser pulses in the modulating wiggler magnets, where the interaction occurs, must be smaller than the duration of the electron bunch. Otherwise, laser pulses will simply miss the electron beam from time to time and the x-ray signal in these cases will have only the pedestal and no AXP. On the other hand, if the timing jitter is smaller than the duration of the electron bunch, one can improve the contrast of the AXP by lowering the pedestal using emittance spoiling techniques suggested in [18] over the edges of the electron bunch [19]. Synchronization to the laser pulse is important for pump-probe experiments where the laser pulse (or any other signal derived from the laser pulse) is used as a pump and the AXP is used as a probe.

III. SIMULATION RESULTS

The radiation produced by the modulated, bunched electron beam has been simulated using the FEL code GENESIS [20]. Electron beam and undulator parameters are as in Sec. II. The undulators are planar with period 3 cm, and 89% of the FEL beam line is filled with undulators, with quadrupoles in the gaps to form a FODO lattice.

First, we briefly examine an example corresponding to a single modulating laser as in Fig. 4(a). The main current spike, with 17 kA peak current and a FWHM of 360 attoseconds (as), reaches saturation after passing through 50–60 m of the undulator. After 50 m, there is roughly $7 \mu\text{J}$ of energy in this pulse, which has a FWHM of 250 as in terms of power. The width of the radiation produced by this current spike is prevented from becoming smaller by the slippage between the radiation field and the electron beam; over a typical gain length, the slippage is roughly 60 as. A typical profile of the output power after 50 m is shown in Fig. 6. The closest side peaks to the main current peak produce a smaller but comparable amount of peak power; in terms of total x-ray energy, the contribution from the two side peaks is roughly the same as that from the central peak. Thus, in experiments using this radiation, the short width of the individual pulses will tend to be obfuscated by the separation between pulses, which is determined by the 1200 nm (or 4 fs) period of the modulating laser.

We now consider the radiation produced by an electron beam which has been modified through interacting with two laser pulses, at 1200 and 1600 nm wavelengths, in two separate single-period undulators. The resulting current profile is contrasted with the current profile obtained using a single-laser pulse and modulating undulator in Fig. 7. While the central peak is roughly similar to the single-laser case, with 18 kA maximum current and a FWHM of 480 as, the side peaks are significantly reduced in current,

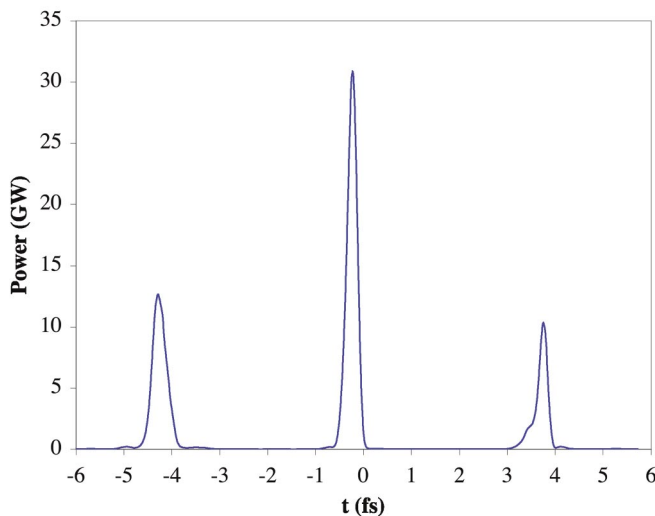


FIG. 6. (Color) An example of the x-ray power profile produced when using a single modulating laser, after 50 m.

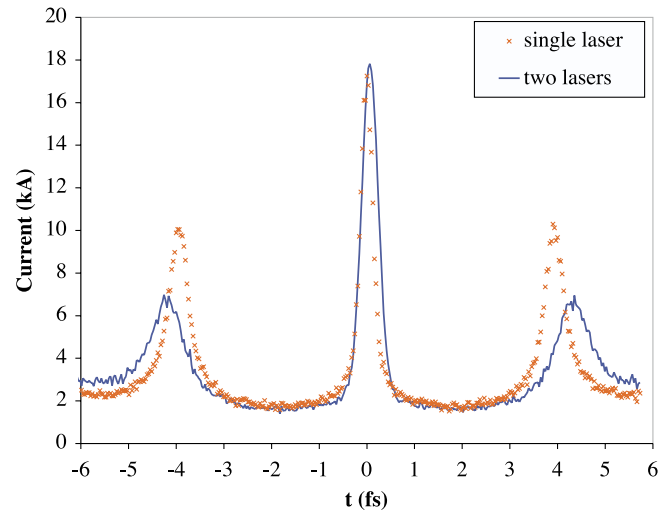


FIG. 7. (Color) Current profiles resulting from interaction with two separate lasers (line) and with a single laser (\times).

reaching 7 kA instead of 10 kA. The main current spike, as well as the secondary peaks in current produced by these beam manipulations, were simulated up to 20 times using different random seeds for the shot noise within the electron beam. The radiation from the high-current region displays, at best, a gain length of 3.9 m until it reaches saturation levels after passing through around 50–60 m of the FEL. The typical peak power after 50 m is 40 GW. At this point, the x-ray energy produced by the current spike grows very slowly, and only because slippage lengthens the pulse width. The only significant side peaks are 4 fs away from the central peak, and have a gain length of 5.2 m. The difference in gain length is sufficient to delay by 10 m the point at which the radiation from these sections of the electron beam reaches saturation levels.

The unperturbed part of the electron beam has a gain length of 12 m during the first 40 m of the undulator, although the growth rate does begin to accelerate after 40 m. After the beam has passed through 60 m of the undulator, the SASE process reaches its maximum growth rate with gain length of 6.0 m. For an electron bunch length of 100 fs, the energy of background x rays produced by the bulk of the beam after 50 m is $6.1 \mu\text{J}$, which is only slightly below the x-ray energy produced by the current spike.

The dependence on the x-ray energy from the main current peak, two of the side peaks, and the background are shown as a function of distance along the FEL in Fig. 8. The background level is slowly growing, although it starts at a larger level due to the significantly larger duration of the entire pulse. The energy from the main density peak consistently only exceeds the background energy between 40 and 55 m. The energy from the side peaks are only comparable to the background near 50 m. At this point, the main pulse is already approaching saturation levels. The contrast ratio in terms of x-ray energy of the main current

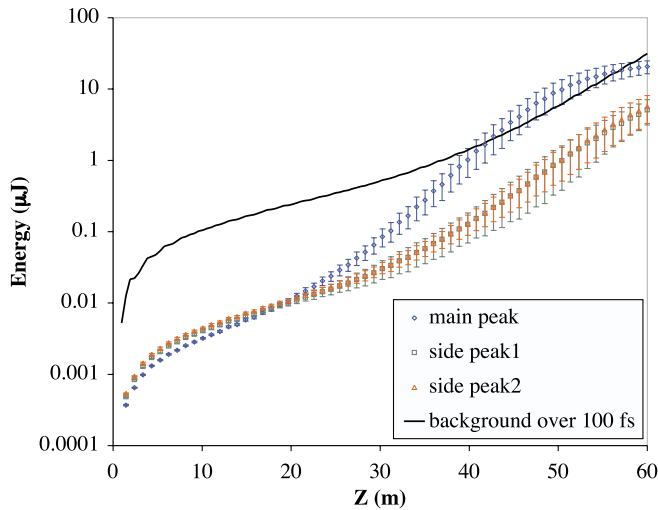


FIG. 8. (Color) Expected x-ray energy produced from various sources (the central current peak, the side peaks, and the background) as a function of distance along the undulator. Variations in energy due to shot noise are indicated by the error bars.

peak compared with the energy from the side peaks and from 100 fs of unperturbed beam is shown as a function of distance in Fig. 9. The main peak has by far the highest peak power, but because of its short duration the contrast ratio remains of order unity.

After 50 m of undulator, the background energy from the bulk of the beam is $6.1 \mu\text{J}$. The main peak averages $9.8 \mu\text{J}$ per energy while each side peak averages about $1 \mu\text{J}$ of energy. Each x-ray pulse exhibits roughly 40% variation between simulations which use different random seeds for the shot noise. The total contrast ratio between the main current peak and the combined sources of radiation from

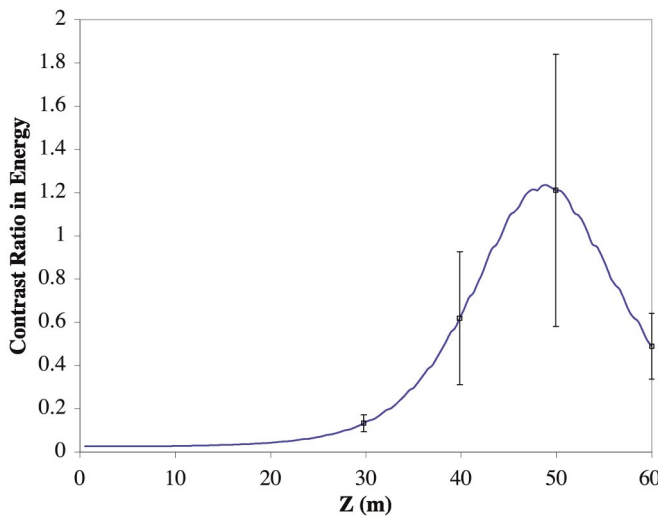


FIG. 9. (Color) Contrast ratio in terms of x-ray energy between the main current peak and the rest of the electron beam, including side peaks. Statistical fluctuations in the contrast ratio are indicated for several locations in z .

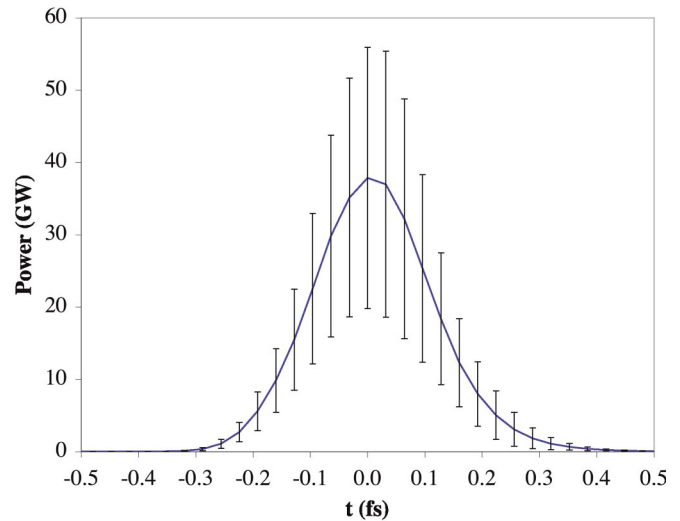


FIG. 10. (Color) Time dependence of the average radiation power, with statistical deviations arising from different random seeds for the shot noise.

the rest of the beam is approximately 1:1. This is an improvement over the contrast ratio of approximately 0.5:1 for the case where a single laser is used.

The statistics for the power profile of the main pulse are summarized in Fig. 10. The large fluctuations are a result of variations in both the total energy per pulse and changes in the temporal pulse shape. Two example pulses are illustrated in Fig. 11. The width of individual pulses, measured as the FWHM in power, is on average 250 as, with a standard deviation of 50 as. The power profile can have either one or two peaks. The location of the peaks fluctuates significantly, but always by less than 250 as from the average location.

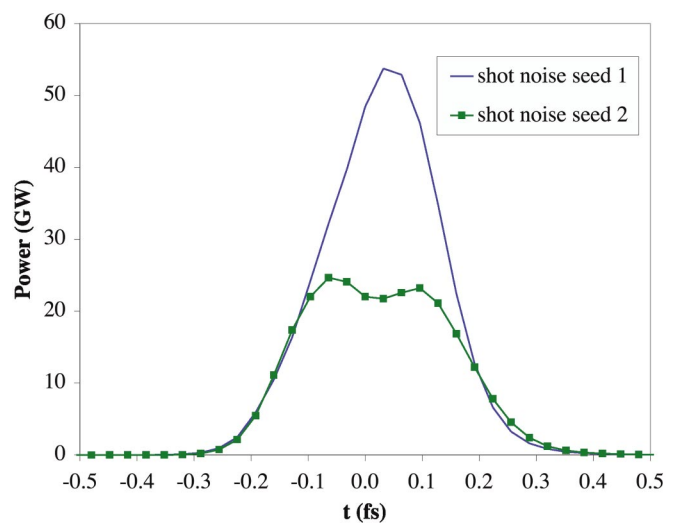


FIG. 11. (Color) Time dependence of the radiation power for the central density spike, resulting from two different random seeds for shot noise.

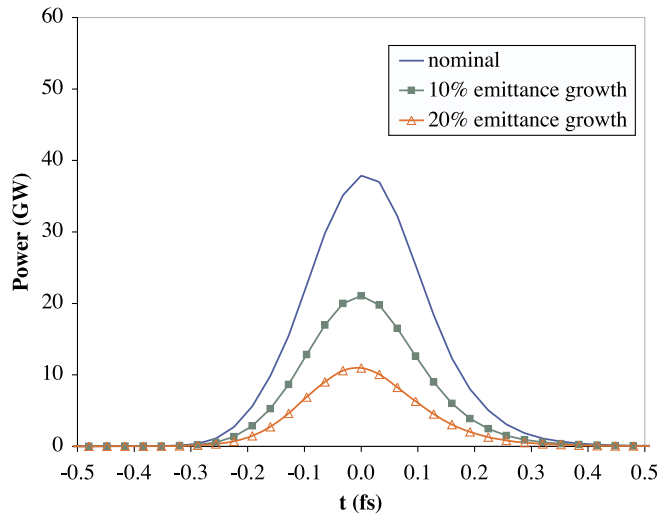


FIG. 12. (Color) Average temporal profile of beam power from the main peak in current, for different normalized emittances.

One area of concern for this technique is that the region of enhanced current may experience an increase in transverse emittance in the chicane. This would counteract the reduction in gain length caused by the increase in peak current. To assess the severity of this effect, we have simulated the x-ray output from the main current peak for different values of the transverse emittance. In Fig. 12, the nominal case of $1.2 \mu\text{m}$ emittance is compared with similar beams that suffer 10% or 20% emittance growth. We observe that these two examples reduce the average energy per pulse, and thus the contrast ratio, by factors of 1.9 and 3.6, respectively.

An additional concern for implementing such a technique is in synchronizing the separate interactions of the electron beam with the 1200 and 1600 nm laser pulses. A change in relative timing will alter the envelope of the energy modulation experience by the beam, and will tend to enhance the radiation produced by the side peaks in current. One can moderate this effect by using a common source signal to produce the 1200 and 1600 nm laser pulses.

IV. CONCLUSIONS

A technique has been described for producing ~ 250 as x-ray pulses using an FEL at close to saturation power levels. This is achieved by manipulating the beam so as to enhance the FEL gain rate over a very short time interval of the electron beam. The combination of interacting with a few-period laser while passing through a single-period undulator, followed by passage through a dispersive section, creates an enhancement in instantaneous current over a very short time scale. To maintain the central current peak as the dominant source of x rays, it has proved desirable to include two separate modulation sections to produce a single, distinct peak. One section uses a 1200 nm laser, while the other uses a 1600 nm laser to

create an effective waveform having a larger bandwidth than is practical using a single laser.

While some questions remain concerning synchronization of two laser pulses and possible degradation of beam quality during the microbunching process, simulations indicate that this is a promising method to achieve subfemtosecond x-ray pulses. Furthermore, this method has the advantage of boosting the FEL performance of the target region of the electron beam, so that the total undulator length required to reach saturation is reduced, in this case to 50 m.

The enhanced performance of the current peak, with a factor of 5 enhancement over the average current, is sufficient to create a significant increase in the FEL output from this portion of the electron beam. Assuming a bunch length of 100 fs, and taking into account the FEL output from smaller current peaks produced by this method, the x rays from the current peak stand out from the background with a contrast ratio of 1:1; in other words, on average 50% of the photons coming from the electron beam fall within a single pulse having FWHM of 250 as. Simulations indicate shot-to-shot fluctuations of 40% in the number of photons from this pulse.

ACKNOWLEDGMENTS

This work was supported by the Director, Office of Science, of the U.S. Department of Energy under Contract No. DE-AC03-76SF00098.

-
- [1] E. L. Saldin, E. A. Schneidmiller, and M. V. Yurkov, *Opt. Commun.* **212**, 377 (2002).
 - [2] A. A. Zholents and W. M. Fawley, *Phys. Rev. Lett.* **92**, 224801 (2004).
 - [3] E. L. Saldin, E. A. Schneidmiller, and M. V. Yurkov, *Opt. Commun.* **237**, 153 (2004).
 - [4] E. L. Saldin, E. A. Schneidmiller, and M. V. Yurkov, *Opt. Commun.* **239**, 161 (2004).
 - [5] A. A. Zholents, *Phys. Rev. ST Accel. Beams* **8**, 040701 (2005).
 - [6] Y. Kobayashi and K. Torizuka, *Opt. Lett.* **26**, 1295 (2001).
 - [7] X. Fang and T. Kobayashi, *Opt. Lett.* **29**, 1282 (2004).
 - [8] C. P. Hauri, P. Schlup, G. Arisholm, J. Biegert, and U. Keller, *Opt. Lett.* **29**, 1369 (2004).
 - [9] A. Baltuška, T. Fuji, and T. Kobayashi, *Opt. Lett.* **27**, 1241 (2002).
 - [10] W. B. Colson, in *Laser Handbook* (North-Holland, Amsterdam, 1990), Vol. 6, Chap. 5.
 - [11] J. B. Murphy and C. Pellegrini, in *Laser Handbook* (Ref. [10]), Vol. 6, Chap. 2.
 - [12] A. Amir and Y. Greenzweig, *Nucl. Instrum. Methods Phys. Res., Sect. A* **250**, 404 (1986).
 - [13] C. Pellegrini, *Nucl. Instrum. Methods Phys. Res., Sect. A* **475**, 1 (2001).
 - [14] J. Arthur *et al.* (LCLS Design Study Group), SLAC Report No. SLAC-R-521, 1998.

- [15] A. A. Zholents, W.M. Fawley, P. Emma, Z. Huang, G. Stupakov, and S. Reiche, in *Proceedings of the 2004 FEL Conference (FEL2004)*, pp. 582–585, available online at <http://www.JACoW.org>.
- [16] Z. Huang and T. Shaftan, Nucl. Instrum. Methods Phys. Res., Sect. A **528**, 345 (2004).
- [17] M. Xie, Nucl. Instrum. Methods Phys. Res., Sect. A **445**, 59 (2000).
- [18] P. Emma *et al.*, Phys. Rev. Lett. **92**, 074801 (2004).
- [19] As recommended by P. Emma (private communication).
- [20] S. Reiche, Nucl. Instrum. Methods Phys. Res., Sect. A **429**, 243 (1999).